Available online at www.sciencedirect.com
ScienceDirect
Journal of Power Sources 160 (2006) 1403–1409
JOURNAL OF POWER SOURCES
www.elsevier.com/locate/jpowsour

Charge and discharge characteristics of a commercial $LiCoO_2$-based 18650 Li-ion battery

S.S. Zhang *, K. Xu, T.R. Jow

U.S. Army Research Laboratory, AMSRD-ARL-SE-DC, Adelphi, MD 20783-1197, USA

Received 13 February 2006; received in revised form 8 March 2006; accepted 8 March 2006
Available online 2 May 2006

Abstract

We studied the charge and discharge characteristics of commercial $LiCoO_2$-based 18650 cells by using various electrochemical methods, including discharging at constant power, ac impedance spectroscopy, and dc-voltage pulse. At 20 °C, these cells deliver 8.7–6.8 Wh of energy when discharged at a power range of 1–12 W between 2.5 and 4.2 V. Ragone plots show that the effect of discharge power on the energy is significantly increased with decreasing of the temperature. For example, energy of the cell is entirely lost when the temperature downs to −10 °C and the discharge rate still remains at 10 W. Impedance analyses indicate that the total cell resistance (R_{cell}) is mainly contributed by the bulk resistance (R_b, including electric contact resistance and electrolytic ionic conductivity), solid electrolyte interface resistance (R_{sei}), and charge-transfer resistance (R_{ct}). Individual contribution of these three resistances to the cell resistance is greatly varied with the temperature. Near room temperature, the R_b occupies up to half of the cell resistance, which means that the rate performance of the cell could be improved by modifying cell design such as employing electrolyte with higher ionic conductivity and enhancing electric contact of the active material particles. At low temperature, the R_{ct}, which is believed to reflect cell reaction kinetics, dominates the cell resistance. In addition, galvanosatic cycling tests indicate that the charge and discharge processes have nearly same kinetics. The performance discrepancy observed during charging and discharging, especially at low temperatures, can be attributed to these two factors of: (1) substantially higher R_{ct} at the discharged state than at the charged state; (2) asymmetric voltage limits pre-determined for the charge and discharge processes.
Published by Elsevier B.V.

Keywords: 18650 Li-ion battery; Charge; Discharge; Constant power; Impedance; Low temperature

1. Introduction

The 18650 Li-ion battery is one of the preferable choices for the efficient mobile power sources in many military applications, such as objective force warrior (OFW) and future combat system (FCS), because of its cylindrical configuration favorable for high energy storage and easy thermal management [1,2]. Such a battery, featuring a cylindrical configuration with a diameter of 18 mm and a length of 65 mm, usually has a rated capacity of 1.5–2.6 Ah, which depends on the cell chemistry and the targeted power-energy balance [3–21]. Normally, high power design requires thin electrodes and preferably has an enhanced content of the electrochemically inert conducting agent (carbon black), which adversely leads to a slightly low energy density. Since the 18650 battery has the similar design (including safety protecting components) as these heavy-duty Li-ion batteries used in electric vehicle (EV) and hybrid electric vehicle (HEV), many researchers have used it as the testing vehicle to evaluate new battery materials and cell safety characteristics [3–5] or to diagnose mechanism of cell performance fading [6–11].

In the view of cell performance, much of effort has been focused on the evaluation of charge and discharge performance and of electrochemical characteristics [12–21]. It has been reported that power and energy of a Li-ion battery are significantly decreased as the temperature downs to −20 °C or lower [15,17,18]. For example, the delivered power and energy densities of a commercial 18650 Li-ion battery at −40 °C fall to <10 W l^{-1} and ∼5 Wh l^{-1}, respectively, from ∼800 W l^{-1} and ∼100 Wh l^{-1} at 25 °C [15]. These results are based on an experiment, in which the battery was normally charged at room temperature and discharged at low temperature. The ac impedance and dc polarization analyses have indicated that such losses are

* Corresponding author. Tel.: +1 301 394 0981; fax: 1 301 394 0273.
E-mail address: szhang@arl.army.mil (S.S. Zhang).

0378-7753/$ – see front matter. Published by Elsevier B.V.
doi:10.1016/j.jpowsour.2006.03.037

attributed to the substantially increased interfacial resistance between the cathode and electrolyte, instead of the decreased ionic conductivity of the electrolyte [15,17]. Apparently, there is a significant discrepancy in the cycling performance between charge and discharge at low temperatures, which has never been studied except that we analyzed and discussed on a small button cell [22,23]. At low temperatures (<−10 °C), charging Li-ion battery is strictly restricted although it can be normally discharged with a reasonable loss in the power and energy. Part of the reasons is due to plating of metallic lithium, which could cause safety concern. Our recent study showed that even if the plating of metallic lithium occurs, the plated lithium may immediately react with graphite to form lithium graphite compound [24], which effectively suppresses the formation of dendrite lithium. Therefore, we consider that charging Li-ion cell at low temperature could be allowable as long as the current is not high.

In this work, we used various electrochemical techniques to evaluate the charge and discharge characteristics of commercial $LiCoO_2$-based 18650 cells. Our focus was on understanding the performance discrepancy between the charge and discharge processes. We used ac and dc methods to measure cell impedance and discussed limitation to the cycling performance at low temperatures and compared the cell resistance results by ac impedance and dc-pulse polarization methods.

2. Experimental

Commercial 18650 cells with $LiCoO_2$ as the active cathode material were evaluated. The product data sheet shows that this model of cells has a rated capacity of 2.4 Ah and an averaged discharge voltage of 3.75 V when cycled at 21 °C between 2.5 and 4.2 V. Three cells with a weight of 47 ± 0.2 g were tested under the same conditions and the data with middle performance was collected to plot. A Tenney Environmental Oven Series 942 was used to provide a constant temperature environment for all tests. Before testing at each temperature, the cells were rested for 6 h to reach thermal equilibrium between the oven and cell inside components.

A Maccor Series 4000 tester was employed for cycling tests. Unless otherwise described, the cell was charged at 20 °C by a constant-current/constant-voltage (CC–CV) protocol. That is, the cell was charged at 0.5 C until the voltage reached to 4.2 V, followed by holding the voltage at 4.2 V until the current dropped to 0.05 C. Solartron SI 1287 Electrochemical Interface and SI 1260 Impedance/Gain-Phase Analyzer were adopted for ac impedance measurements and dc pulse tests. To describe state-of-discharge (DOD) of the cell, we defined it as the ratio of discharging capacity at a specific point to the capacity obtained at 20 °C by discharging at 0.5 C from fully charged state to 2.5 V. For the measurement of impedance at various DOD, the experiment was started from the charged state. The cell was discharged at 0.05 C to a specific DOD and left the cell rest for 1 h to reach a stable open-circuit voltage (OCV), and then the impedance was measured by applying a 5 mV of ac oscillation over the frequency range from100 kHz to 0.01 Hz. Repeating this procedure until the cell was discharged to 2.5 V. More details about the testing conditions will be described in Section 3. The ac impedance spectra and dc polarization curves recorded by Solartron were fitted using ZView and CorrView software, respectively (Scribner and Associates, Inc.).

3. Results and discussion

3.1. Discharging performance at constant power

In this work, we used a constant power (CP) protocol to evaluate discharge performance of the 18650 cells since many electronic devices require a CP supplier and the data based on a CP condition may provide more accurate information for such devices. Fig. 1 shows a typical CP discharge profile of the 18650 cells, in which the power is constantly controlled at 8 W by adjusting voltage and current instantly. With discharging, the voltage slowly declines while the current changes in the opposite way. Near the end of discharge, the current is dramatically increased to compensate for the voltage drop, which consequently raises ohm polarization and advances the end of discharge. Therefore, it would be normal that the discharge capacity (Ah) by the CP protocol is slightly lower than that by the normal CC protocol.

Fig. 2 shows the effect of discharge power on the delivered energy for an 18650 cell. At 20 °C, the cell delivers 8.64 Wh of energy at a discharge rate of 2 W, and the energy gradually decreases with increasing the power (Fig. 2a). For example, the energy falls to 6.77 Wh when the power increases to 12 W. At low temperature (−20 °C, Fig. 2b), the effect of discharge power on the energy becomes more significant. It can be seen from Fig. 2b that at low power (0.3 W), the cell is able to deliver 8.05 Wh energy, however, it drops to 0.99 Wh as the power increases to 8 W. To observe effect of the temperature on discharge energy, we plotted discharge voltage curves at 4 W and at different temperatures in Fig. 3. It is shown that the energy is significantly declined with the temperature decreasing, especially when the temperature is below 10 °C.

Results of Figs. 2 and 3 are summarized in Fig. 4 by plotting cell power against the energy. This type of plots is called "Ragone plot", which has been long used in the battery community to compare various kinds of power sources [25]. Fig. 4 indicates that high power and high energy of the cell can be achieved only at 20 °C. Even at 10 °C, the energy suffers signif-

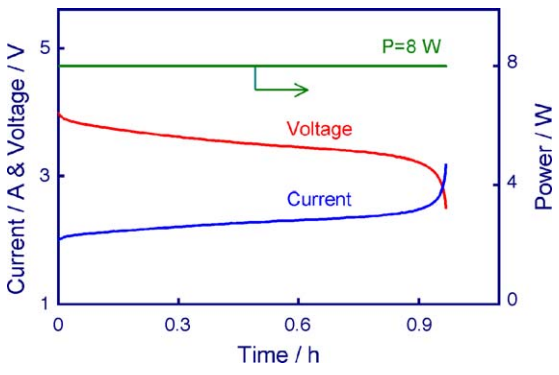

Fig. 1. A typical discharge protocol of an 18650 Li-ion cell at a constant power (8 W).

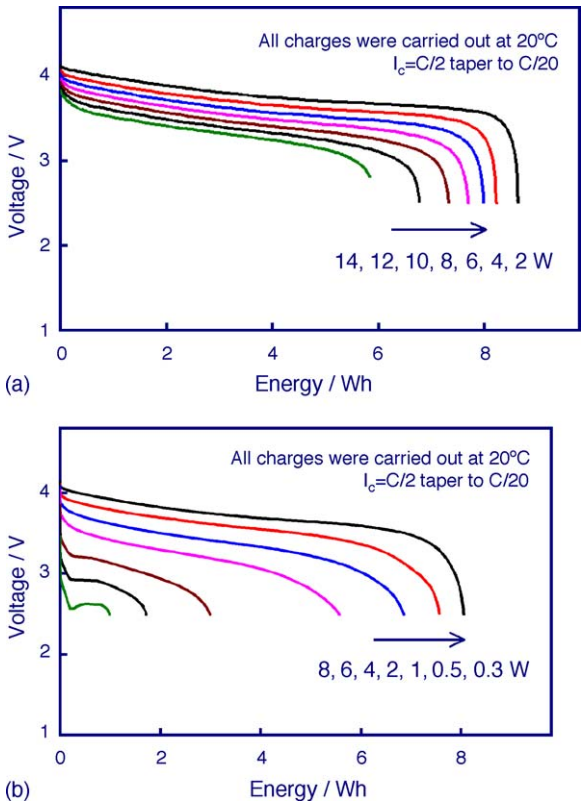

Fig. 2. Discharge voltage curves of an 18650 cell at different powers. (a) 20 °C and (b) −20 °C.

icant loss as the power increases to 10 W or higher. For example, the energy is decreased by about half as the power is increased from 2 to 10 W. On the other hand, the energy becomes more sensitive to the power with the temperature decreasing. At −10 and −20 °C, the cell entirely fails to deliver energy as the power remains at 10 W whereas it is able to deliver up to full energy at low power (<0.5 W). The above facts indicate that the best operating temperature toward the optimized energy and high power is near 20 °C or slightly higher. At low temperatures, utilization of the energy is dramatically decreased with increasing of the power. For use at low temperatures, the Li-ion cell is more attractive in the case needing low power.

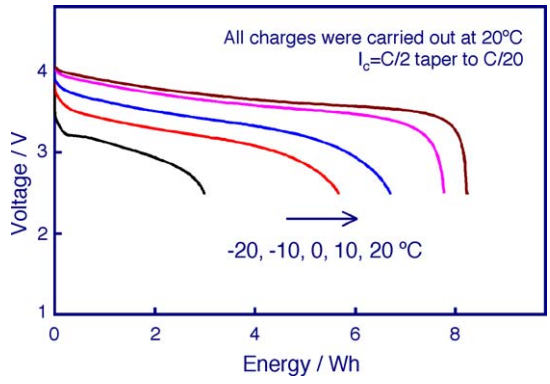

Fig. 3. Effect of temperature on the discharge energy of an 18650 cell, in which the data was recorded at 4.0 W.

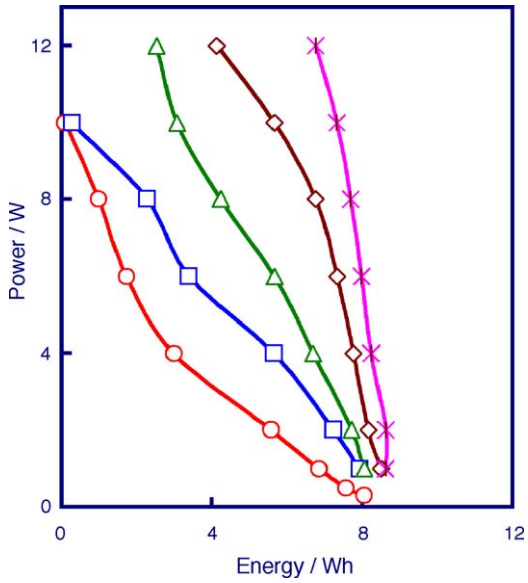

Fig. 4. Ragone plots of an 18650 cell at 20 °C (×), 10 °C (◊), 0 °C (△), −10 °C (□), and −20 °C (○).

Fig. 5 displays the effect of discharge protocol on the cycling life of the 18650 Li-ion cell, in which the same CC–CV schedule was used for all charges. The cell was first cycled for 175 times using a 0.5 C of CC discharge protocol, followed by a 4 W of CP discharge protocol for the rest of cycles. According to the energy (8.24 Wh at 20 °C) of the cell, these two protocols should generate similar discharge time (rate). However, the CP discharge protocol resulted in slower capacity fading than the normal CC discharge. This merit may be attributed to the dramatic increase in the current near the end of discharge (see Fig. 1), its resulting ohm polarization promotes the cell voltage reaching the pre-determined voltage limit to end discharge. This effect is equivalent to lifting of the discharge voltage limit, which is believed to be helpful for extending cycling life of the Li-ion batteries.

3.2. Impedance analysis

Ac impedance was used to study low temperature characteristics of the Li-ion cell. A typical impedance spectrum of the 18650

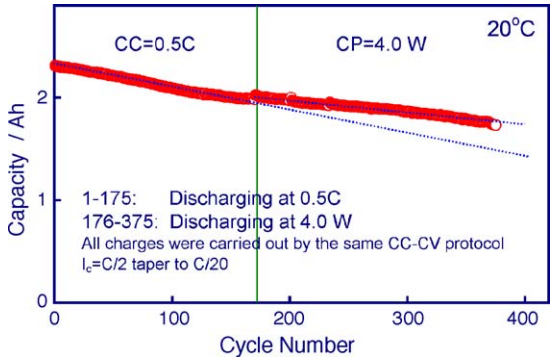

Fig. 5. Effect of discharge protocols on the cycling life of an 18650 cell, in which the cell was charged using a normal CC–CV schedule and discharged using different protocols.

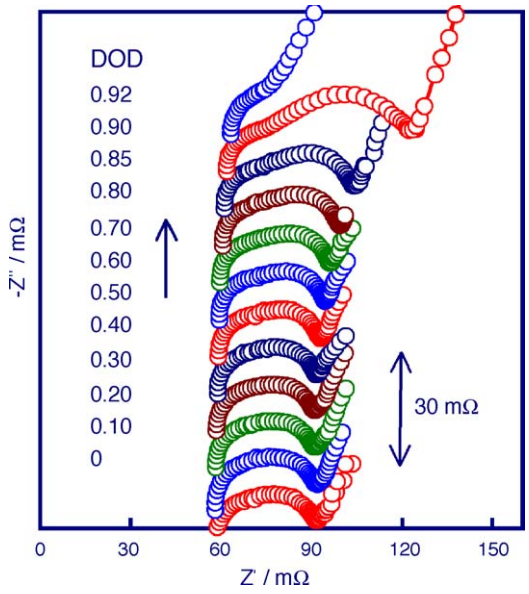

Fig. 6. Impedance spectra of an 18650 cell at different DOD, which were recorded at 20 °C.

cells shows an inductive loop at very high frequency followed by two over-lapped semicircles through high to middle frequency and a straight sloping line at low frequency. The inductive loop at very high frequency is changed with the cell design and electrode structure, and in the case of 18650 cells it could be attributed to the jelly-roll configuration, porous electrode structure, and safety protecting components if any [14]. By deleting the inductive loop, we plotted impedance spectra of the 18650 cell at various DOD in Fig. 6, which shows that all impedance spectra belong to the above descriptions except for the one with a DOD of 0.92. Such impedance patterns can be interpreted in terms of bulk impedance, interfacial impedance and Faradic impedance. The bulk impedance could be a pure ohm resistance (R_b), which reflects electronic and ionic resistance of two electrodes and electrolyte/separator. The interfacial impedance, which corresponds to the semicircle at high frequency, could be attributed to resistance (R_{sei}) and capacitance (C_{sei}) of the solid electrolyte interface formed on the surface of two electrodes. Faradic impedance consists of charge-transfer impedance and Warburg impedance. The charge-transfer impedance, which corresponds to the semicircle at medium frequency, could be attributed to charge-transfer resistance (R_{ct}) and its related double-layer capacitance (C_{dl}). Warburg impedance, which corresponds to the straight sloping line at low frequency, could be related to diffusion of lithium ions on the interface between the active material particles and electrolyte.

Individual values of the R_b, R_{sei}, and R_{ct} for the impedance spectra of an 18650 cell with different DOD at 20 and −20 °C, respectively, were fit using Zview software and were plotted as a function of the DOD in Fig. 7. To discuss cell total resistance (R_{cell}), we defined it as the value of the intercept at lower frequency of the R_{ct} semicircle and real resistance axis. As indicated in Fig. 7a and b, the R_b and R_{sei} are independent of the DOD, whereas the R_{ct} changes a lot with the DOD, which hence causes R_{cell} change. The unchanged R_{sei} is attributed to a result

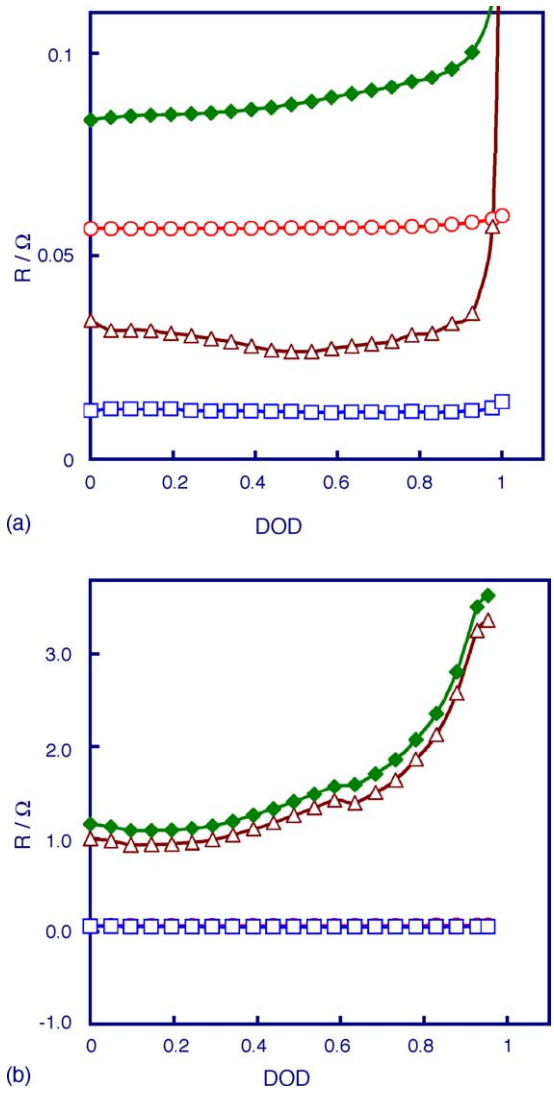

Fig. 7. Contribution of the R_b (◯), R_{sei} (□), and R_{ct} (△) to the R_{cell} (♦) for an 18650 cell at various DOD. (a) 20 °C and (b) −20 °C. Note that R_b and R_{sei} in (b) are overlapped with each other.

of the combined effect of two opposite changes of the cathode and graphite with the DOD [22]. Fig. 7a shows that at 20 °C, the individual resistances are changed in the order of $R_b > R_{ct} > R_{sei}$, and that the R_b occupies more than half of the R_{cell}. This fact suggests that reducing R_b could be effective in improving the rate performance of the 18650 Li-ion cells, which normally could be achieved by improving electric contact and choosing electrolyte with higher ionic conductivity. At −20 °C (Fig. 7b), the resistance order is changed to $R_{ct} \gg R_{sei} \approx R_b$, and in this case the R_{cell} is dominated by the R_{ct}. This result suggests that reducing the R_{ct} could be the most effective approach to improving the low temperature performance of the Li-ion cells. On the other hand, we noticed that the R_{ct} at discharged state (DOD = 1) is much higher than at charged state (DOD = 0). This is one of the reasons why charging a Li-ion cell from the discharged state is relatively difficult while the opposite discharging is much easier.

Fig. 8 plots "log(1/R)" as a function of the "1/T" for the 18650 cell with a DOD of 0.40. It is interesting to note that the plots for

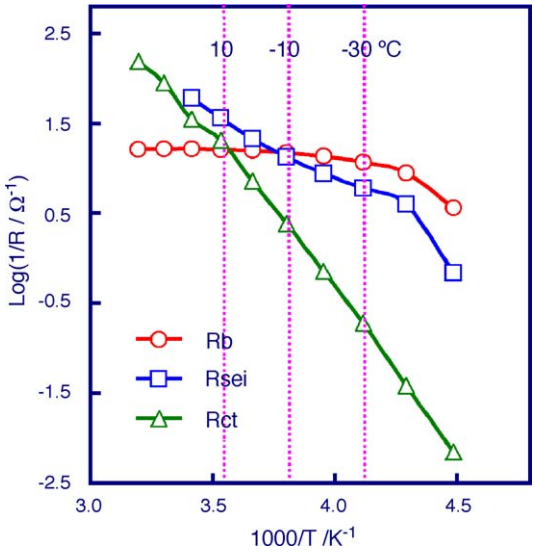

Fig. 8. Temperature dependence of the R_b, R_{sei}, and R_{ct} of an 18650 cell at a DOD of 0.40.

R_b and R_{sei} exhibit a Vogel–Tammann–Fulcher behavior (VTF, being a curve) whereas that for R_{ct} presents an Arrhenius behavior (being a straight line). Based on the fact that VTF behavior is characteristic of the ionic conductivity in a non-crystalline solid or a liquid, and "1/R" has the same physical meaning as the ionic conductivity (both use the unit of Ω^{-1}), we consider that the R_b and R_{sei} are most likely related to the ionic conductivity of the liquid electrolyte/separator and the interfacial surface layers. On contrary, Arrhenius behavior suggests that the R_{ct} could be linked to the kinetics of cell reaction. Among the above three resistances, the R_{ct} is most sensitive to the temperature. One can see from Fig. 8 that the R_{ct} is comparable with the R_b and R_{sei} above −10 °C, however, it rapidly increases with decreasing of the temperature. As a result, the R_{ct} becomes the predominant factor to limit low temperature performance of the Li-ion cells.

To confirm the meaning of the R_{ct}, we plotted it together with differential capacity of the cell versus the cell voltage in Fig. 9. It is obvious that both the R_{ct} and differential capacity show two board peaks, and these two peaks appear in the same

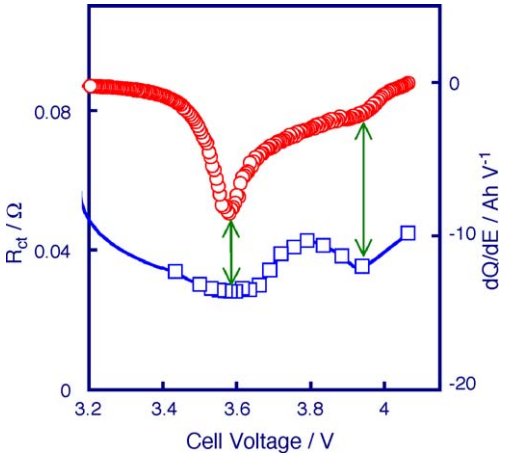

Fig. 9. Correlation of the R_{ct} (□) and differential capacity (◯) of the 18650 cell.

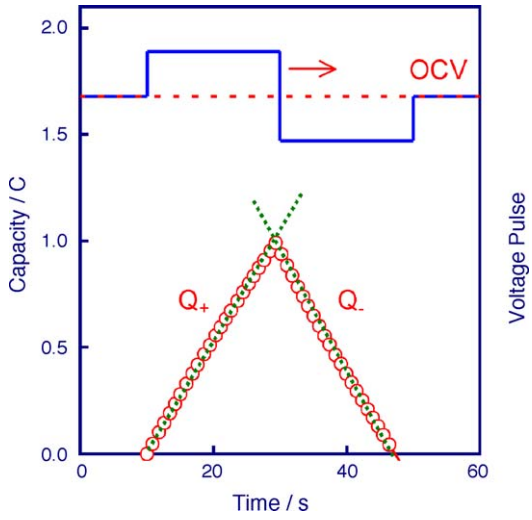

Fig. 10. Testing protocol for a ±10 mV, 20 s voltage pulse and its resulting response of the capacity with respect to the time.

voltage regions. It has been reported that the differential capacity, or alternatively a cyclic voltammogram, is closely related to the diffusivity of lithium ions for the intercalation and de-intercalation with the $LiCoO_2$ cathode [26] and graphite anode [27]. The excellent consistence between the R_{ct} peaks and differential capacity peaks verifies that the R_{ct} must be associated with the kinetics of the cell reaction.

3.3. dc pulse analysis

A dc pulse method was further used to analyze the charge and discharge characteristics of the 18650 cells. The same procedures, as described in the experimental for ac impedance measurements, but with the dc pulse test replacing impedance measurement were used for this purpose. Fig. 10 illustrates the testing protocol of the dc-voltage pulse experiment. At a certain DOD (certainly with stable OCV), a +10 mV voltage pulse was first applied to the cell for 20 s followed by reversing the pulse polarity to −10 mV for another 20 s, during which the response of capacity (i.e., the number of coulombs) with respect to the time was recorded. Since the cell has large capacity (2.28 Ah at 20 °C) and the voltage pulse is very small, the Q–t response presents a very good straight-line correlation (see Fig. 10). The slope of Q–t response reflects an average current during the positive (charge) and negative (discharge) pulse, respectively. Therefore, the individual resistance of the charge and discharge process, respectively, at a certain DOD can be calculated using the following equation:

$$R = \frac{E}{\text{Slope}} \tag{1}$$

where E is 10 mV for both of the charge and discharge pulses. In addition, the averaged dc resistance of the cell is given by the following equation:

$$R_{dc} = \frac{2E}{\text{Slope}_+ + \text{Slope}_-} \tag{2}$$

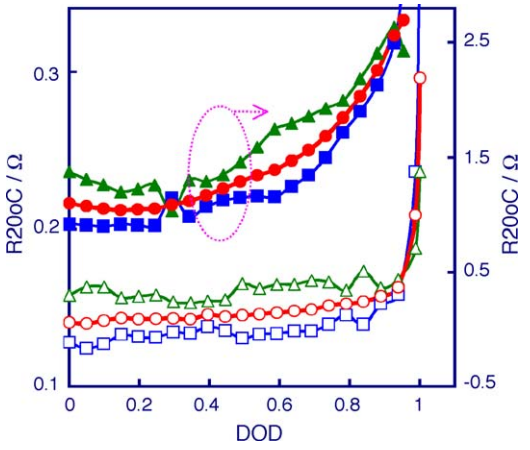

Fig. 11. Charge resistance (squares), discharge resistance (triangles), and the averaged cell resistance (circles) of an 18650 cell as a function of the DOD at 20 °C (in hollow symbols) and −20 °C (in solid symbols), respectively.

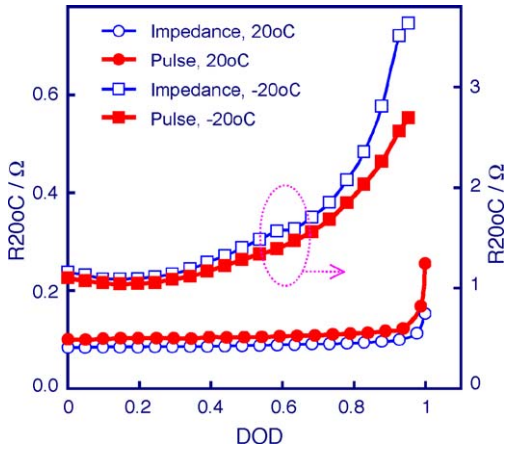

Fig. 12. Comparison of the cell resistances measured by ac impedance and dc-voltage pulse method, respectively.

where the Slope_+ and Slope_- are the absolute value obtained from Fig. 10.

Individual resistances of the charge and discharge processes as well as the averaged dc resistance are plotted versus the DOD in Fig. 11, which shows that the discharged state has much higher resistance than the charged state. This observation is in good agreement with the ac impedance results as discussed above. Comparing the charge and discharge resistances with each other, one finds that the charge resistance is always slightly lower than the discharge resistance. To confirm this result, we conducted the following experiments: (1) changing the order of pulse polarity from ±10 to ∓10 mV; (2) using current pulse (±5 and ∓5 mA, respectively), instead of the voltage pulse; (3) repeating pulse tests in the charge process, instead of in the discharge process. All the above experiments led to very similar results only with error range variations. Therefore, the result that the charge resistance is slightly lower than the discharge resistance is reliable and reproducible although it apparently conflicts with the normal impression that the charging process is more difficult than the discharging process for the Li-ion cells.

3.4. Comparison of the ac impedance and dc pulse methods

Normally, resistance results by ac and dc methods are very difficult to be compared with each other since the dc results strongly depend on the height and width of the pulse applied. When a high pulse (i.e., high voltage for the voltage pulse or high current for the current pulse) is applied, the cell's DOD might be changed a lot even if the time is very short, which could increase the complication of the test. In such a case, significant difference in the resistance results between charge (or so-called Regen) and discharge could be obtained [28]. In the present work, we used a small voltage pulse (±10 mV), and hence its results are well comparable with the ac impedance data (Fig. 12). As shown in Fig. 12, the resistance results by ac impedance and dc-voltage pulse are very consistent with each other except for these at −20 °C and with high DOD (>0.80). Both methods verify that the Li-ion cells show much higher resistance at discharged state than at charged state, and the ac impedance analyses reveal that this phenomenon is due to the strong voltage (or DOD) dependence of the R_{ct}.

3.5. "Apparent" performance discrepancy between charge and discharge

Beside the much higher R_{ct} at discharged state than at charged state, the asymmetric voltage limits pre-determined for cycling is another source to result in an "apparent" performance discrepancy between the charge and discharge. To show this, we plotted OCV of the 18650 cell and voltage limits for the cycling in Fig. 13, in which the OCV was recorded after the cell was discharged to a certain DOD followed by resting for 1 h to reach a stable reading. The voltages allowable for polarization of the charge (U_{Ch}) and discharge (U_{Disch}) are given by Eqs. (3) and (4), respectively:

$$U_{Ch} = 4.2 - \text{OCV} \tag{3}$$

$$U_{Disch} = \text{OCV} - 2.5 \tag{4}$$

where 4.2 and 2.5 V are the pre-determined voltage limits for the charge and discharge, respectively. Obviously, the U_{Ch} and U_{Disch} are significantly asymmetric and their difference changes with the DOD, as shown in Fig. 13 by the lines with an arrow in

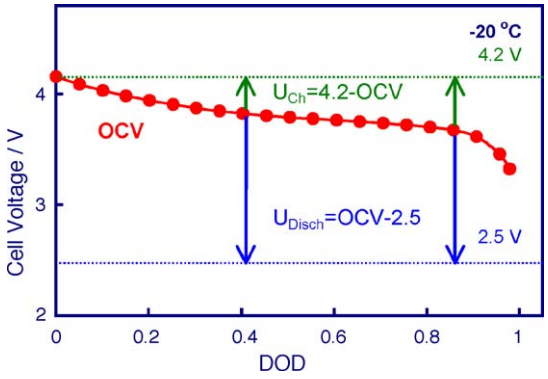

Fig. 13. Plots of the charge and discharge voltage limits versus OCV of an 18650 cell.

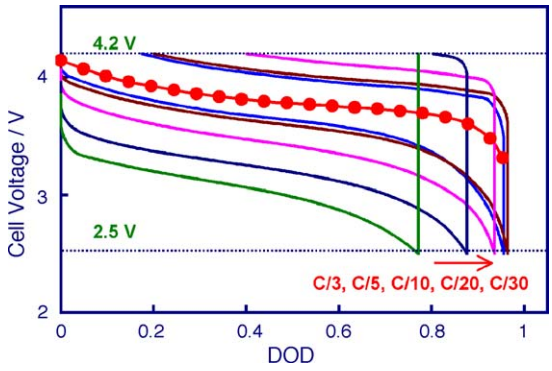

Fig. 14. Charge and discharge voltage curves of an 18650 cell at different current rates and at −20 °C, in which the curve with solid circle symbols represents OCV of the cell at −20 °C.

one end. It is the asymmetric voltage limits (i.e., $U_{Ch} < U_{Disch}$) that result in "apparent" discrepancy in the performance of the charge and discharge. To support this conclusion, we conducted discharge–charge cycling tests at −20 °C, and plotted the voltage curves in Fig. 14. In this experiment, the test was started with discharging the cell from the charged state (pre-charged at 20 °C) and rested for 1 h after the end of discharge, followed by charging the cell at the same current rate. Let us observe the actual polarization voltage of the charge (U_{Ch}) and discharge (U_{Disch}) processes at the same DOD, that is

$$U_{Ch} = U_{Cell} - OCV \quad (3)$$

$$U_{Disch} = OCV - U_{Cell} \quad (4)$$

where U_{Cell} is the actual voltage of the cell during charging and discharging, respectively. It is clear that the U_{Ch} and U_{Disch} at the same DOD are nearly identical. This result further verifies that the charge and discharge processes of the Li-ion cell have same kinetics, and that the asymmetric voltage limit is one of the important factors to result in the "apparent" performance discrepancy between charge and discharge, especially at low temperature. In addition, Fig. 14 shows that CC-charging Li-ion cell at −20 °C is possible if the current rate is very low (for example, *C*/30 and *C*/20). When the current increases to *C*/3, the CC-charge is ended immediately by the pre-determined upper voltage limit whereas under the same conditions the cell can discharge up to a DOD of 0.77.

4. Conclusions

From the results of this work, the following conclusions might be made on the $LiCoO_2$-based 18650 Li-ion cells. (1) The combined benefit of the high power and energy densities can be well utilized only near 20 °C or slightly higher. (2) At low temperatures, the cell is able to deliver high energy but loses a lot of power. (3) Poor low temperature performance of the cell is due to the substantially increased R_{ct}, which is attributed to relate to slow kinetics of the cell reactions. (4) The R_{ct} is strongly dependent of the cell's DOD and it is much more sensitive to the temperature than the R_b and R_{sei}. (5) Analyses of the impedance results suggest that the approaches to improving power performance should be focused on reducing R_b for near room temperatures and on reducing R_{ct} for low temperatures. (6) At all temperatures, the charge and discharge have nearly same kinetics. (7) The "apparent" performance discrepancy between the charge and discharge, especially at low temperatures, is due to these two facts of (a) the R_{ct} at discharged state is much higher than that at charged state and (b) the pre-determined asymmetric voltage limit is more favorable for the discharge process.

References

[1] E.J. Plichta, M.A. Hendrickson, R.P. Hamlen, Proceedings of the IEEE 17th Annual Battery Conference on Applications and Advances, Long Beach, CA, January 15–18, 2002, p. 109.
[2] G. Au, L. Cristo, D. Bennington, A. Pellegrino, Proceedings of the IEEE 17th Annual Battery Conference on Applications and Advances, Long Beach, CA, January 15–18, 2002, p. 63.
[3] E.V. Thomas, H.L. Case, D.H. Doughty, R.G. Jungst, G. Nagasubramanian, E.P. Roth, J. Power Sources 124 (2003) 254.
[4] D.P. Abraham, J. Liu, C.H. Chen, Y.E. Hyung, M. Stoll, N. Elsen, S. MacLaren, R. Twesten, R. Haasch, E. Sammann, I. Petrov, K. Amine, G. Henriksen, J. Power Sources 119–121 (2003) 511.
[5] D. Zhang, B.S. Haran, A. Durairajan, R.E. White, Y. Podrazhansky, B.N. Popov, J. Power Sources 91 (2000) 122.
[6] P. Ramadass, B. Haran, R. White, B.N. Popov, J. Power Sources 111 (2002) 210.
[7] P. Ramadass, B. Haran, R. White, B.N. Popov, J. Power Sources 112 (2002) 606.
[8] P. Ramadass, B. Haran, R. White, B.N. Popov, J. Power Sources 112 (2002) 614.
[9] G. Ning, B. Haran, B.N. Popov, J. Power Sources 117 (2003) 160.
[10] G. Sikha, P. Ramadass, B.S. Haran, R.E. White, B.N. Popov, J. Power Sources 122 (2003) 67.
[11] A.T. Stamps, C.E. Holland, R.E. White, E.P. Gatzke, J. Power Sources 150 (2005) 229.
[12] B.A. Johnson, R.E. White, J. Power Sources 70 (1998) 48.
[13] J.P. Fellner, G.J. Loeber, S.S. Sandhu, J. Power Sources 81–82 (1999) 867.
[14] G. Nagasubramanian, J. Power Sources 87 (2000) 226.
[15] G. Nagasubramanian, J. Appl. Electrochem. 31 (2001) 99.
[16] G. Nagasubramanian, D.H. Doughty, J. Power Sources 150 (2005) 182.
[17] J. Fan, J. Power Sources 117 (2003) 170.
[18] J. Fan, J. Power Sources 138 (2004) 288.
[19] K. Sit, P.K.C. Li, C.W. Ip, C.W. Li, L. Wan, Y.F. Lam, P.Y. Lai, J. Fan, D. Magnuson, J. Power Sources 125 (2004) 124.
[20] E.P. Roth, D.H. Doughty, J. Power Sources 128 (2004) 308.
[21] I. Bloom, A.N. Jansen, D.P. Abraham, J. Knuth, S.A. Jones, V.S. Battaglia, G.L. Henriksen, J. Power Sources 139 (2005) 295.
[22] S.S. Zhang, K. Xu, T.R. Jow, Electrochim. Acta 49 (2004) 1057.
[23] S.S. Zhang, K. Xu, T.R. Jow, Electrochim. Commun. 4 (2002) 928.
[24] S.S. Zhang, K. Xu, T.R. Jow, J. Power Sources 160 (2006) 1349–1354.
[25] D.V. Ragone, Mid-Year Meeting of the Society of Automotive Engineers on Review of Battery Systems for Electrically Powered Vehicles, Detroit, MI, May 20–24, 1968.
[26] K. Dokko, M. Mohamedi, Y. Fujita, T. Itoh, M. Nishizawa, M. Umeda, I. Uchida, J. Electrochem. Soc. 148 (2001) A422.
[27] M. Umeda, K. Dokko, Y. Fujita, M. Mohamedi, I. Uchida, J.R. Selman, Electrochim. Acta 47 (2001) 885.
[28] I. Bloom, S.A. Jones, V.S. Battaglia, G.L. Henriksen, J.P. Christophersen, R.B. Wright, C.D. Ho, J.R. Belt, C.G. Motloch, J. Power Sources 124 (2003) 538.